Synthesis and Characterization of the Mesoporous Silicate Molecular Sieve MCM-48

Antonio A. Romero,[†] María D. Alba,[‡] Wuzong Zhou, and Jacek Klinowski*

Department of Chemistry, University of Cambridge, Lensfield Road, Cambridge CB2 1EW, U.K.

Received: January 6, 1997; In Final Form: March 25, 1997[⊗]

We have used powder X-ray diffraction, diffuse reflectance Fourier-transform infrared, ^{29}Si MAS NMR, N_2 adsorption, and transmission electron microscopy to examine the role of the concentration of silica, the surfactant, and the reaction time in the synthesis of high-quality silica mesoporous molecular sieve MCM-48. The XRD patterns of the products are consistent with the hexagonal → cubic → lamellar phase transformation.

Introduction

The discovery of the M41S family of mesoporous molecular sieves[1,2] has expanded the range of uniform pore sizes from the microporous (<13 Å, as found in zeolites) into the mesopore range (>20 Å) and generated considerable interest in open-structured inorganic materials. Three subgroups of the family have been reported: a hexagonal phase referred to as MCM-41, a cubic phase (space group *Ia*$\bar{3}$*d*) known as MCM-48, and MCM-50, an unstable lamellar phase.[3,4]

The procedures used for the preparation of mesoporous silica materials are similar to those in the synthesis of zeolites,[5] except that a surfactant instead of an inorganic base or an amine is used as the template.[1,2] Mesoporous silica is made under mild hydrothermal conditions (typically below 120 °C) in the presence of anionic, cationic, or neutral surfactants, under either basic or acidic conditions.[6−10] Aware that the atomic arrangement in these materials is not crystalline, we shall refer to "crystallinity" in the sense of the regular arrangement of uniform channels, the only element of order. All references to a unit cell, etc., should be interpreted accordingly.

Surfactant chemistry is the key to the formation of mesoporous silica. The silicate species in solution play an important role in the organization of the surfactant molecules,[11,12] and the electrostatic interaction between the inorganic and surfactant ions determines the morphology of the mesophase.[1,2,6,11−13] Solid-state NMR helps to elucidate the nature of the three major processes involved in the synthesis:[14−17] (1) assembly of the surfactant system and the formation of ion pairs between polydentate and polycharged inorganic species; (2) self-organization of ion pairs into a mesophase with a liquid-crystal structure (hexagonal, lamellar, or cubic), the nature of which depends on the composition of the mixture, the pH, the temperature, and the reaction time;[4] (3) polycondensation of the silicate species leading to the formation of a rigid structure.

Interest in the mesoporous silica sieves has been concentrated almost exclusively on MCM-41,[1−10] and very little information is available on MCM-48.[18,19] The aim of this work is to give a comprehensive overview of the parameters controlling the synthesis of the MCM-48: the concentration of silica at constant surfactant concentration, the degree of the OH^-/halide ion exchange of the surfactant, the nature of the halide (Br^- or Cl^-), and the duration of the synthesis.

TABLE 1: Synthesis Conditions for the Formation of the Mesoporous Products. The Degree of Hydroxyl Exchange of the Surfactant Is Given in Parentheses

material	surfactant	Sfct/Si	synthesis method
I-B30-1.2	CTAB/OH (30%)	1.2	I
I-C40-0.8	CTAC/OH (40%)	0.8	
II-C30-0.8	CTAC/OH (30%)	0.8	II
II-C30-1.0		1.0	
II-C30-1.2		1.2	
II-C35-0.8	CTAC/OH (35%)	0.8	
II-C35-1.0		1.0	
II-C35-1.2		1.2	
II-C40-0.8	CTAC/OH (40%)	0.8	
II-C40-1.0		1.0	
II-C40-1.2		1.2	

Experimental Section

Synthesis. The source of silica was tetraethylorthosilicate (TEOS) from Aldrich. The surfactants were cetyltrimethylammonium chloride (CTAC) and bromide (CTAB) [$C_{16}H_{33}(CH_3)_3NX$, X = Cl or Br] (Aldrich). $C_{16}H_{33}(CH_3)_3NX$/OH was prepared by batch exchange of a 25 wt % aqueous $C_{16}H_{33}(CH_3)_3NX$ solution with the IRA-420(OH) ion-exchange resin (Aldrich). The degree of exchange of hydroxide for halide ion was 30%, 35%, or 40%.

TEOS was added slowly under constant stirring to a solution of CTAC or CTAB in various proportions to give the desired surfactant/silica (Sfct/Si) molar ratio. The mixture was then stirred for 1 h at room temperature. Two different synthesis procedures were then used. In method I the reaction mixture was transferred into Teflon bottles and placed into a furnace at 110 °C for 48 h to give MCM-48.[7] In method II, which allows sampling at different reaction times in order to monitor the appearance of intermediate phases, the reaction mixture was transferred into round-bottom Pyrex flasks and heated in a silicone oil bath at 120 °C. In both methods, the ethanol produced in the hydrolysis of the TEOS was allowed to evaporate. Part of the water was removed from the gel mixture in the same way, so that the gel mixture became more concentrated in the course of the reaction. When water was prevented from evaporating from the gel mixture, only MCM-41 was obtained. Table 1 shows the Sfct/Si ratio, the nature of the CTAX/OH solution (50 mL), and the synthesis method. The solid products were recovered by filtration, washed with distilled water, dried in air at 75 °C overnight and then calcined at 550 °C for 24 h in air. The designation of each sample is composed

* Telephone: +(44)−1223−33 65 14. FAX: +(44)−1223−33 63 62. E-mail: jk18@cam.ac.uk

[†] On leave from: Departamento de Química Organica, Universidad de Córdoba, San Alberto Magno s/n, 14004 Córdoba, Spain.

[‡] On leave from: Departamento de Química Inorganica, Instituto Ciencia de los Materiales, Universidad de Sevilla, C. S. I. C., P. O. Box 874, 41012 Sevilla, Spain.

[⊗] Abstract published in *Advance ACS Abstracts,* June 15, 1997.

S1089-5647(97)00077-1 CCC: $14.00

of three segments separated by hyphens. The first gives the synthesis procedure (method I or method II); the second gives the nature of the surfactant (B for cetyltrimethylammonium bromide and C for chloride) and the degree of OH^-/Br^- or OH^-/Cl^- exchange; the third gives the Sfct/Si ratio. Thus I-B30-1.2 signifies a sample made using method I with 30% hydroxyl-exchanged cetyltrimethylammonium bromide and Sfct/Si = 1.2.

Sample Characterization

Powder X-ray Diffraction (XRD). XRD patterns were recorded using a Philips 1710 powder diffractometer with Cu Kα radiation (40 kV, 40 mA), a step size of 0.02°, and a 1 s counting time per step.

Diffuse Reflectance Fourier-Transform Infrared (DRIFT). DRIFT spectra were recorded on a Bomem MB-100 instrument equipped with an "environmental chamber" (Spectra Tech, P/N 0030-100) placed in the diffuse reflectance attachment (Spectra Tech, Collector). The resolution was 8 cm^{-1}, and 256 scans were averaged to obtain spectra in the 4000−400 cm^{-1} range. Single-beam spectra were measured with the spectra of KBr or of as-synthesized MCM-48 acquired at the same temperature as the sample. The temperature was measured by inserting a thermocouple directly into the sample. Calcined samples were dried at 150 °C for 48 h, diluted with KBr to 10 wt %, placed in an environmental chamber cell with a 20 mL min^{-1} flow of dehydrated deoxygenated nitrogen, heated to 300 °C, and held at this temperature for 1 h prior to measuring the spectrum. In DRIFT characterization of template removal, the experiments were carried out in air. As-synthesized MCM-48 was diluted to 10 wt % in KBr and equilibrated for 1 h at 100 °C prior to the collection of the spectra (against KBr and MCM-48 reference spectra). The sample was then heated to 300 °C and held at this temperature for 1 h prior to measuring the spectrum (against the KBr reference spectrum). Afterwards, the temperature was lowered to 100 °C and stabilized for 1 h before the difference spectrum (against as-synthesized MCM-48 as a reference) was measured.

Magic-Angle-Spinning (MAS) NMR. ^{29}Si MAS NMR spectra were acquired at 79.4 MHz with 90° radiofrequency pulses and 600 s recycle delays using a Chemagnetic CMX-400 spectrometer and zirconia rotors 7.5 mm in diameter spun in air at 4 kHz. $^1H-^{29}Si$ cross-polarization (CP) MAS spectra were recorded with a single contact pulse sequence with 8 ms contact time, 11.5 μs ^1H 90° pulse, 4 s recycle time, and 700 scans. The Hartmann−Hahn condition was established using a sample of kaolinite, and the chemical shifts are given in ppm from external tetramethylsilane (TMS).

Nitrogen Sorption. N_2 adsorption/desorption isotherms were measured at 77 K with a Micromeritics Instrument Model ASAP 2000. The samples were outgassed at 200 °C for 28 h. The volume of adsorbed N_2 was normalized to standard temperature and pressure. The BET surface area was calculated applying the BET equation for the relative pressure between 0.05 and 0.3. The *t*-plots were drawn to evaluate the microporosity by comparing the shape of a given isotherm with that of a standard on a nonporous solid, which has been selected here according to IUPAC recommendation.[20] The pore size distribution (PSD) was calculated using the adsorption branch of the N_2 adsorption/desorption isotherm and the Barrett−Joyner−Halenda (BJH) formula.[21] The cumulative pore volume, V_{BJH}, and the cumulative surface area, A_{BJH}, of the mesopores were obtained from the PSD curve.

Transmission Electron Microscopy (TEM). Calcined samples were dried at 400 °C for 2 h. After being cooled to room temperature in a dry container, the anhydrous powder was deposited on a copper grid with a holey carbon film and rapidly transferred to a JEOL JEM-200CX electron microscope operating at 200 kV. The sample was then kept in the microscope vacuum (ca. 5×10^{-7} Torr) overnight. TEM images were recorded at magnifications from 24000× to 75000× depending on the beam stability of the specimen.

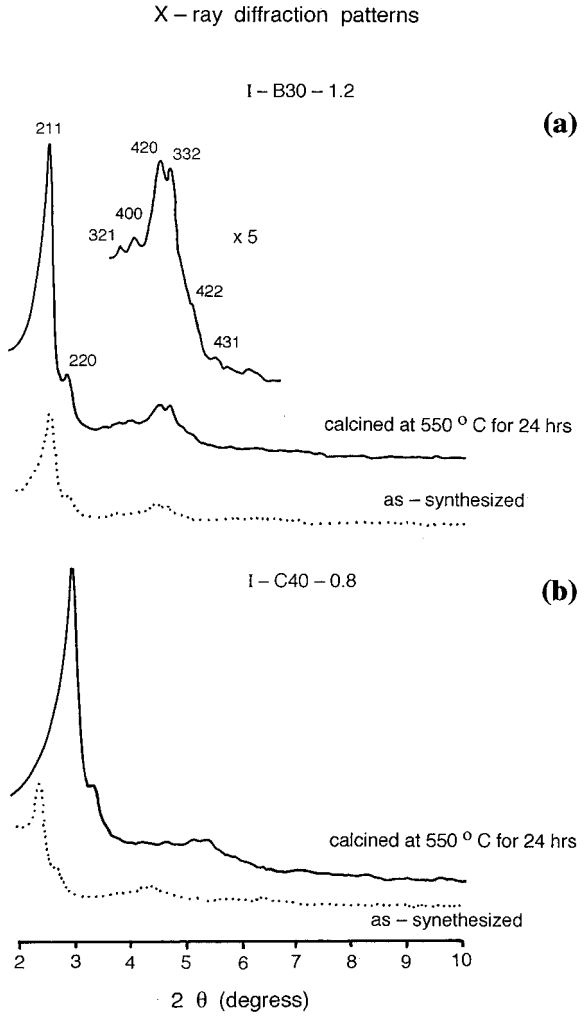

Figure 1. Powder X-ray diffraction patterns of samples (a) I-B30-1.2 and (b) I-C40-0.8. Dotted lines denote patterns of as-synthesized materials; solid lines, patterns of samples calcined at 550 °C for 24 h.

Results and Discussion

XRD. The powder X-ray diffraction patterns of the products of method I (Figure 1) feature distinct Bragg peaks in the range $2\theta = 2-8°$, which can be indexed to different *hkl* reflections, in good agreement with the patterns from a purely siliceous MCM-48.[1,10] The *d*-spacings are compatible with the cubic $Ia\bar{3}d$ space group.[18,22] The reflections from calcined samples are more intense than those of the as-synthesized samples, indicating that the degree of ordering is improved by the removal of the surfactant. Sample I-B30-1.2, prepared with CTAB, is more crystalline than sample I-C40-0.8. The absence of XRD peaks above 10° 2θ indicates that the atomic arrangement within the mesopore walls is disorded.

The cubic unit cell parameters for the as-synthesized samples I-B30-1.2 and I-C40-0.8 are 85.3 and 92.5 Å, respectively (Table 2). Thermal treatment at 550 °C for 24 h is accompanied by a contraction of the unit cell, as can be expected when organic cations are replaced by protons and the adjacent silanol groups condense. However, the contraction of the unit cell in sample I-B30-1.2 (1.3 Å) is more than an order of magnitude smaller

TABLE 2: Cubic Phase Unit Cell Parameter (Å) Calculated as $a = d_{211}\sqrt{6}$. Contraction of the Unit Cell Parameter upon Calcination (in Å) Is Followed (in Parentheses) by the Contraction (in %) with Respect to the Cell Parameter in the As-Synthesized Material

sample	as-synthesized	calcined	contraction
I-B30-1.2	85.3	84.0	1.3 (1.5)
I-C40-0.8	92.5	74.4	18.1 (19.6)
II-C30-0.8	92.3	77.5	14.8 (16.0)
II-C30-1.0[a]	88.3	76.2	12.1 (13.7)
II-C30-1.2[a]	87.3	75.6	11.7 (13.4)
II-C35-0.8[a]	87.9	75.4	12.5 (14.2)
II-C35-1.0[a]	84.9	73.6	11.3 (13.3)
II-C35-1.2[a]	86.3	73.8	12.5 (14.5)
II-C40-0.8[a]	84.2	71.5	12.7 (15.1)
II-C40-1.0[a]	85.3	72.3	13.0 (15.2)
II-C40-1.2[a]	85.4	71.1	14.3 (16.7)

[a] Averaged value.

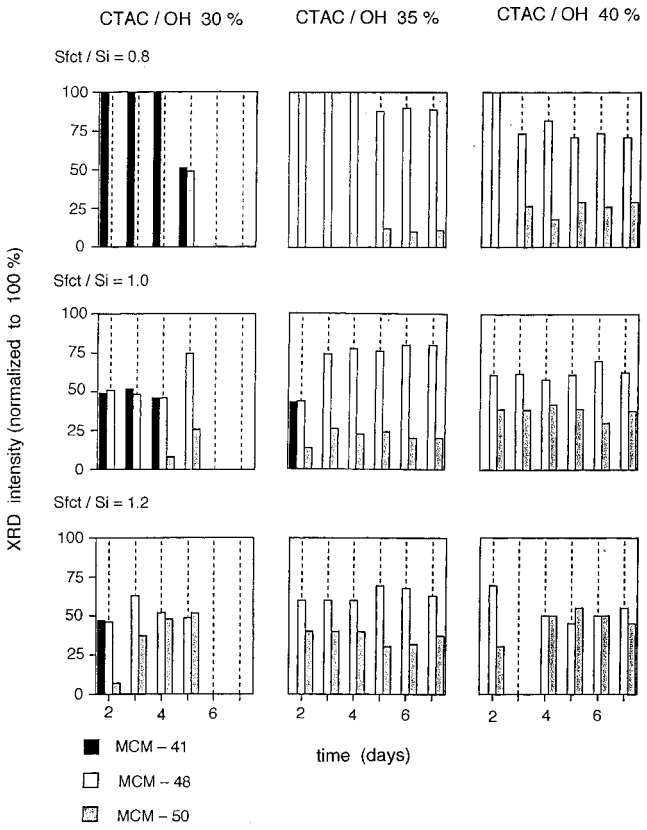

Figure 2. Domains of formation of the hexagonal, cubic, and lamellar phases calculated from the intensity of the XRD patterns as function of synthesis time, Sfct/Si ratio, and the degree of exchange of the hydroxide for the halide ion of the surfactant.

(Table 2) than that reported for a purely siliceous MCM-48 (up to 20 Å[22]). On the other hand, the contraction for sample I-C40-0.8 (18.1 Å) is similar to that previously reported. As the size of the contraction in the unit cell upon calcination is related to the degree of condensation of the product and thus to higher thermal stability, the material obtained using CTAB is expected to be more thermally stable. The higher degree of condensation in sample I-B30-1.2 is clear from the inspection of the ^{29}Si MAS NMR spectra and pore size measurements (see below).

As the XRD patterns were not acquired using the external standard method,[23] the results cannot be used quantitatively. Nevertheless, the presence of three different phases (hexagonal, cubic, and lamellar) in the product of method II can be qualitatively monitored. Figure 2 shows the phase evolution of the products as a function of the duration of the synthesis, the Sfct/Si ratio, and the degree of OH^-/Cl^- exchange in the template. The first product (at short synthesis times) was MCM-41, but we did not detect the presence of a precursor lamellar phase, as reported by Monnier et al.[11] Increased synthesis time gave the trend hexagonal → cubic → lamellar, indicating that increasing gel mixture concentration plays an important role in the organization of the template and the condensation of silanol groups.

For a fixed synthesis time, the nature of the products depends on the Sfct/Si ratio as well as the degree of OH^-/Cl^- exchange in the gel mixture. The formation of the cubic phase is favored at Sfct/Si = 0.8 and the 35% and 40% degree of OH^-/Cl^- exchange after 2 days of reaction at 120 °C.

The values of the cubic unit cell parameters for every composition of the synthesis mixture are given in Table 2. Removal of the surfactant by calcination leads to a contraction of the unit cell by ca. 13 Å. There is similar contraction for method I and similar gel composition.

Diffuse Reflectance Fourier-Transform Infrared (DRIFT). The DRIFT spectrum of as-synthesized sample I-B30-1.2 (1 h at 100 °C, Figure 3a) has no bands in the hydroxyl stretching vibration region (4000−2500 cm^{-1}). There are absorption bands in the stretching region of organic compounds (3000−2800 cm^{-1}) and the bending region (1500−1400 cm^{-1}) for hydrocarbons,[24] both associated with the surfactant. In addition, the spectra show a broad band at ca. 1050 cm^{-1} with a shoulder at 1208 cm^{-1}, characteristic of silica (see below). In contrast, for the as-synthesized sample I-B30-1.2 heated at 300 °C for 1 h in air and cooled to 100 °C, the differential spectrum (Figure 3b) shows a set of bands corresponding to O−H stretching vibrations in the 3000−3800 cm^{-1} range. The appearance of these bands clearly accompanies the removal of the surfactant responsible for the bands at 2929, 2856, and 1470 cm^{-1}. The spectra thus indicate that the surfactant cation balances the charge of the anionic charge, testifying to a strong interaction between the cationic and the silicate species in the as-synthesized samples of MCM-48.

The DRIFT spectrum of as-synthesized I-B30-1.2 recorded (at 300 °C against KBr reference) after treatment at 300 °C for 1 h in air (Figure 3c) shows a band at 3739 cm^{-1} and a broad band at ca. 3600 cm^{-1} assigned to OH stretching. The band at 3739 cm^{-1} is attributed[24] to unassociated silanol groups and the broad band at ca. 3600 cm^{-1} to water and/or bonded silanol groups. The two weak absorption bands at 2940 and 2859 cm^{-1} are associated with residual surfactant. A number of bands are in evidence in the spectra of the skeletal region (below 2500 cm^{-1}): two very weak bands (at 1700 and 1613 cm^{-1}) assigned to H_3O^+ and to the bending mode of H_2O molecules, respectively, a broad band at 1046 cm^{-1} with shoulders at 1235 and 1162 cm^{-1}, and a band at 820 cm^{-1} corresponding to asymmetric and symmetric Si−O stretching vibrations.[25−28] There are also bands at 980 and 600 cm^{-1}, previously assigned[28] to stretching and bending vibrations of surface Si−O$^-$ groups, respectively. The band at 980 cm^{-1} has been reported for crushed silica, silica gels, and zeolites containing a high concentration of defects.[28−30]

All calcined samples give a sharp band at 3739 cm^{-1} arising from isolated Si−OH hydroxyl groups (Figure 3d,e). The Si−OH band from calcined sample I-B30-1.2 (Figure 3d) is more intense than from sample I-C40-0.8 (Figure 3e), indicating a higher population of the OH groups, in agreement with the conclusion from the ^{1}H−^{29}Si CP/MAS NMR spectra (see below). The DRIFT spectra in the 2500−400 cm^{-1} region contain two bands at ca. 1050 (with shoulders at 1227, 1165, and 1127 cm^{-1}) and 820 cm^{-1}, corresponding to asymmetric and symmetric Si−O stretching, respectively. The very weak

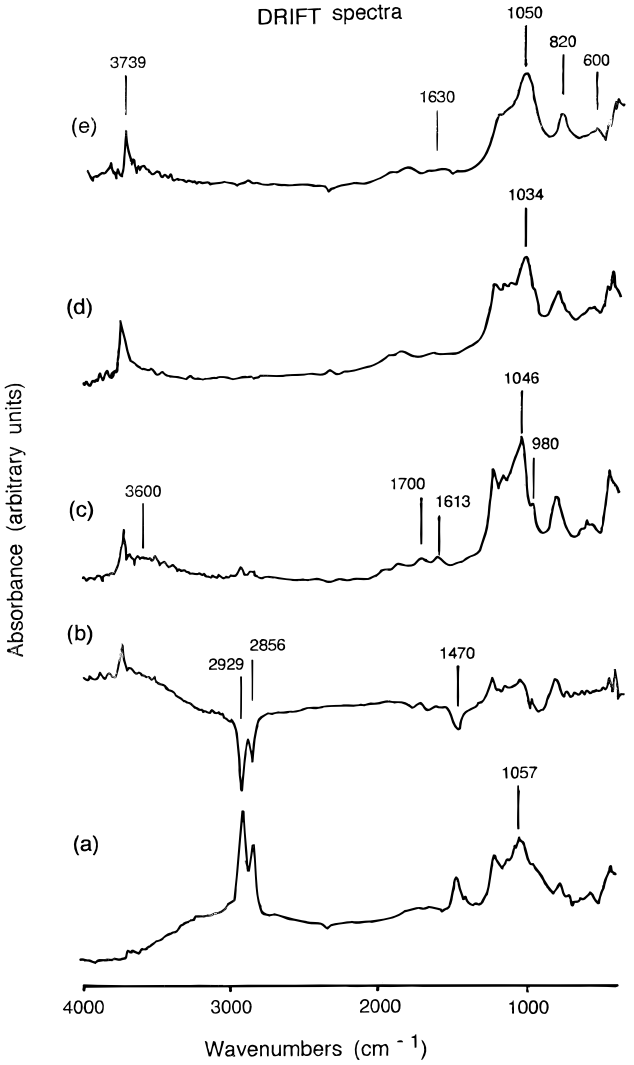

Figure 3. DRIFT spectra of samples I-B30-1.2 and I-C40-0.8. Bands pointing downward are associated with species of decreasing concentration (removal of the template), and bands pointing upward with species formed during calcination. (a) spectrum of as-synthesized sample I-B30-1.2 measured at 100 °C in air against KBr reference. (b) As-synthesized I-B30-1.2. The sample was heated in the spectrometer at 300 °C in air for 1 h, and the spectrum was measured at 100 °C with the as-synthesized sample as reference. (c) Spectrum of as-synthesized sample I-B30-1.2 heated in the spectrometer at 300 °C in air for 1 h. The spectrum was measured at 300 °C against KBr reference. (d and e) Calcined samples I-B30-1.2 and I-C40-0.8, respectively, treated at 300 °C in 20 mL min^{-1} flow of nitrogen for 1 h. The spectrum was measured at 300 °C against KBr reference.

band at ca. 1630 cm^{-1} is associated with the bending mode of H_2O. No spectral features are found at 980 cm^{-1}, where a peak from surface Si−O^- groups would be expected (Figure 3d,e).[28−30] This indicates a high degree of polycondensation. Thus calcination leads to the formation of Si−O−Si bonds via a polycondensation process.

The asymmetric Si−O stretching band from sample I-B30-1.2 shifts to lower wavenumbers as the temperature of treatment increases: 1057 cm^{-1} at 100 °C, 1046 cm^{-1} at 300 °C, and 1034 cm^{-1} (Figure 3a,c,d, respectively). A shift to higher wavenumbers has been reported for SiO_2 glasses[30] and attributed to interparticle sintering. The downward shift in sample I-B30-1.2 thus signifies that such sintering did not occur.

^{29}Si MAS NMR. The "Q^n notation" is often adopted for the description of building units in silicates. In this notation, Q stands for a silicon atom bonded to four oxygen atoms forming a SiO_4 tetrahedron. The superscript n indicates the

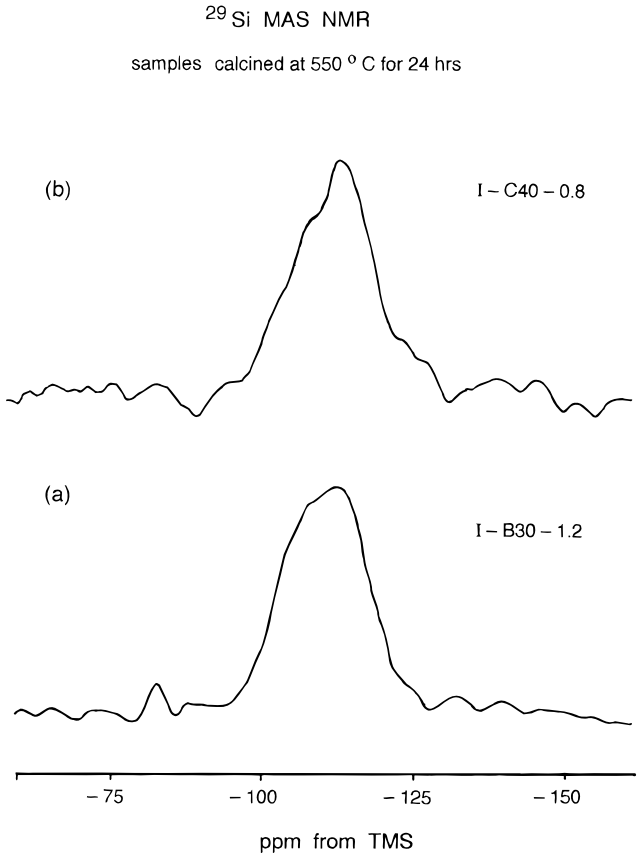

Figure 4. ^{29}Si MAS NMR spectra of calcined purely siliceous samples (a) I-B30-1.2 and (b) I-C40-0.8.

connectivity, i.e. the number of other Q units attached to the unit in question, and the central silicon atom is written in bold. The SiO_4 tetrahedron is 4-connected, and the remaining $(4 - n)$ units linked to it are often hydroxyl groups. Thus, Q^4 stands for three-dimensionally cross-linked **Si**$(OSi)_4$ units, Q^3 for **Si**$(OSi)_3(OH)$ units, and Q^2 for **Si**$(OSi)_2(OH)_2$ units. Polycondensation in silicates is clearly equivalent to the generation of Q^4 units from Q^n units with $n \leq 4$.

The ^{29}Si MAS NMR spectra of the purely siliceous MCM-48 from method I (Figure 4) consist of three broad overlapping peaks from Q^4 silicons (ca. −110 ppm), Q^3 silicons (ca. −101 ppm), and Q^2 silicons (ca. −91 ppm). Given the correlation between the ^{29}Si NMR isotopic chemical shift and the magnitude of the Si−O−Si bond,[31−34] the Q^4 silicons are involved in Si−O−Si angles in the 143.5−168.4° range.

Even given the ca. 8% error inherent in spectral deconvolution, the Q^3/Q^4 population ratio reflects the extent of silanol condensation, indicating a more highly condensed framework in sample I-B30-1.2 ($Q^3/Q^4 = 0.25$) than in sample I-C40-0.8 ($Q^3/Q^4 = 0.45$), in good agreement with an improvement of crystallinity and thermal stability (responsible for the contraction of the unit cell after the removal of the organic) when CTAB is used. In both samples, the degree of condensation of silica is significatly higher than previously reported for high-quality MCM-48.[6,18,35]

^{1}H−^{29}Si CP/MAS spectra (Figure 5) show a marked increase in the relative intensity of the Q^3 line (at −100 ppm) in comparison with the ^{29}Si MAS spectra, confirming that these silicons are attached to hydroxyl groups. This intensity increase is larger for as-synthesized I-C40-0.8 than for as-synthesized I-B30-1.2, where the degree of exchange of hydroxide for halide (and therefore the concentration of OH in the gel mixture) is lower (30% rather than 40%). However, when the surfactant

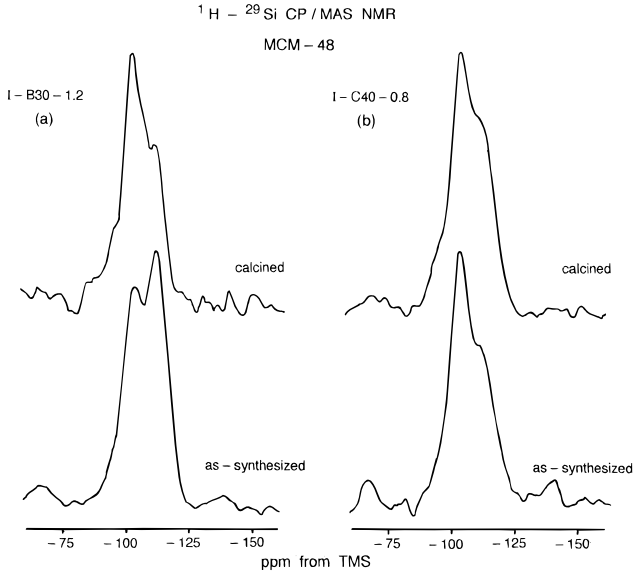

Figure 5. ^{1}H−^{29}Si CP/MAS NMR spectra of calcined samples (a) I-B30-1.2 and (b) I-C40-0.8.

is removed by calcination, the relative intensity of the Q^3 line is higher in sample I-B30-1.2, denoting a higher concentration of silanol groups when CTAB was used. This is in agreement with the DRIFT results.

Nitrogen Adsorption/Desorption Isotherms. The most reliable information about the mesoporous structure of solids comes from low-temperature N_2 adsorption isotherms. Figures 6 and 7 show the amount of nitrogen physisorbed at 77 K versus the relative pressure for samples synthesized by methods I and II. The isotherms are of type IV, typical of mesoporous solids.[36] A well-defined step occurs between $p/p_0 = 0.2$ and 0.3, which is indicative of the filling of the mesopores. The p/p_0 coordinate of the inflection point depends on the pore size. The sharpness in this step suggests a uniform size pore system. The shape of the *t*-plot (not shown) appears to confirm that monolayer−multilayer adsorption has occurred on the pore walls before the onset of capillary condensation at $p/p_0 = 0.2$. Furthermore, the fact that the initial region can be extrapolated back to the origin confirms the absence of any detectable micropore filling at low p/p_0.

The isotherms contain an H3 hysteresis loop as defined by IUPAC,[20] associated with solids with slit-shaped pores or platelike particles. No hysteresis in the adsorption and desorption cycle upon pore condensation was observed in sample I-B30-1.2, the effect related to the small size of the particles as confirmed by TEM. Figure 7 shows that the size of the hysteresis loop increases at long reaction times, which, by the same argument, means that the size of the crystallites has increased.[37]

The BET surface area (Table 3) was calculated[20] with the cross-sectional area of a nitrogen molecule taken as 16.2 Å^2. The results for all samples are in full agreement with the published values.[38] The total volumes of adsorbed N_2, 1.09 cm^3/g for sample I-B30-1.2 and 0.97 cm^3/g for sample I-C40-0.8, are close to the value of 1.02 cm^3/g reported for a purely siliceous highly ordered MCM-48.[22,39]

Plots of the derivative of the pore volume per unit weight with respect to the pore diameter (d*V*/d*D*) versus the pore diameter are shown in Figures 6 and 7. Although the desorption branch is often used for the assessment of the distribution of mesopore sizes, a type H3 hysteresis loop is unlikely to yield a reliable estimate of pore size distribution, even for comparison

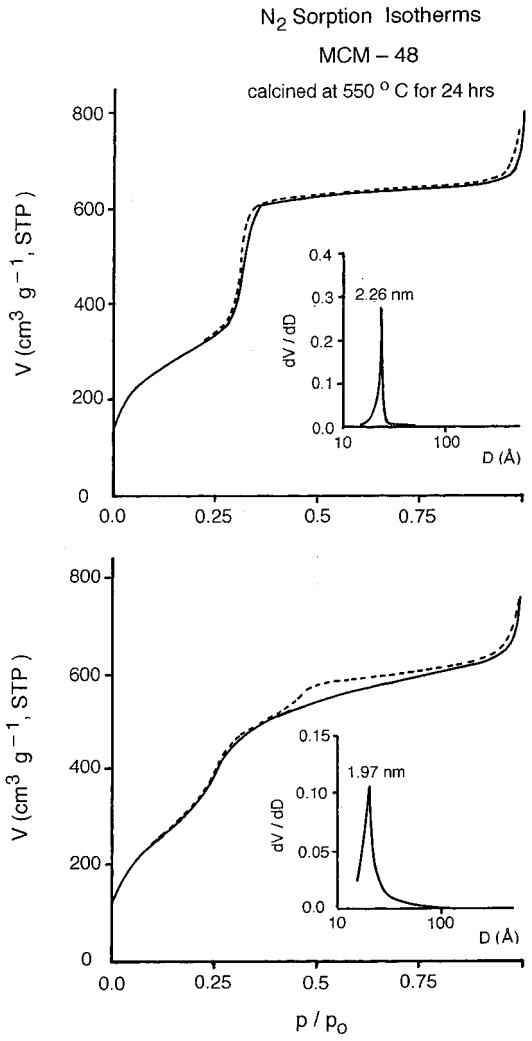

Figure 6. Adsorption (solid line) and desorption (dotted line) isotherms of nitrogen at 77 K on samples (a) I-B30-1.2 and (b) I-C40-0.8. The insets show the pore size distribution calculated from the analysis of the adsorption branch of the isotherms.

purposes.[40] Accordingly, the adsorption branch was used to calculate the mesopore size distribution.

The BJH plot for the physisorption of N_2 on the mesoporous silica materials gives a remarkably narrow pore size distribution with a pore size of ca. 23 Å when CTAB/OH was used as surfactant and ca. 19.5 Å for CTAC/OH. The sharp pore size distribution, with a ca. 5 Å width at half-height, shows that the mesopores are exceptionally uniform.

At long reaction times, the pore homogeneity and the intensity of the maxima in the BJH plot (Figure 7) increase. Although the position of the maxima does not change appreciably, the unit cell parameter increases with time, corresponding to an increased wall thickness with the duration of the synthesis. As can be expected, samples with thicker walls have lower mesopore surface areas.

The pore diameter and unit-cell size in sample I-B30-1.2 are both markedly different from those in other samples. The thicker channel wall corresponds to the particularly high degree of silicate condensation ($Q^3/Q^4 = 0.25$) in this sample. The large unit cell was chosen to satisfy the indices of the XRD peaks.

Transmission Electron Microscopy (TEM). TEM confirms that the structures of the MCM-48 materials prepared by method I are cubic. Figure 8 shows images of the sample I-B30-1.2 viewed down the [100] and [110] zone axes of a cubic unit cell

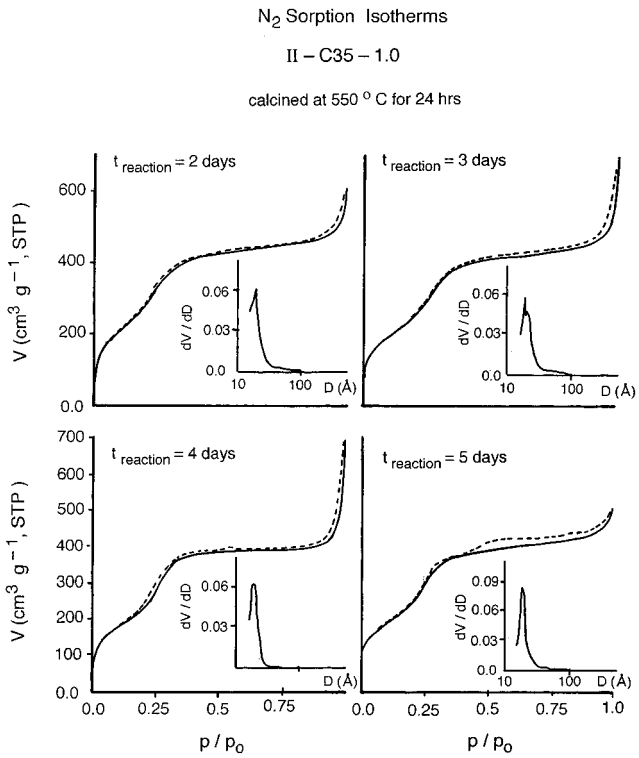

Figure 7. Adsorption (solid line) and desorption (dotted line) isotherms of nitrogen at 77 K on calcined samples II-C35-1.0 at different reaction times. The inset shows the pore size distribution calculated from the analysis of the adsorption branch of the isotherms.

TABLE 3: Cubic Unit Cell Parameter Calculated as $a = d_{211}\sqrt{6}$ and Pore Structure Parameters of the Mesoporous Molecular Sieves Calculated from the Adsorption Branch of the Nitrogen Sorption Isotherm Using the Barrett−Joyner−Halenda Formula

sample	a (Å)	D_{BJH} (Å)	V_{BJH} (cm^3 g^{-1})	A_{BJH} (m^2 g^{-1})	A_{BET} (m^2 g^{-1})
I-B30-1.2	84.0	22.6	1.09	1488	1143
I-C40-0.8	74.4	19.7	0.97	1279	1195
II-C30-1.0					
2 days	74.2	18.4	0.72	936	1490
3 days	75.9	19.4	0.89	938	975
4 days	78.9	19.4	1.01	847	889
5 days	75.9	18.8	0.62	877	1164

with $a = 84$ Å. The [100] image (Figure 8a) is rarely observed.[22] In addition, the image contrast in Figure 8a shows a relatively uneven pattern, suggesting that the principal pore structure is unlikely to be parallel to the ⟨100⟩ zone axis. When viewed down the [110] (Figure 8b) and [111] directions, the images show the pore structure clearly. Indicated by the patterns and contrasts of the TEM images, the space group $Ia\bar{3}d$ can be applied to the MCM-48 structure with a cubic unit cell parameter $a = 84$ Å. A smaller cubic unit cell with $a' = a/\sqrt{2}$ cannot be ruled out. However, one or two weak peaks on the XRD pattern (Figure 1) could not be indexed using this unit cell. Further TEM studies of the local structure of MCM-48 are in progress.

Conclusions

Powder X-ray diffraction, ^{29}Si MAS NMR, N_2 adsorption studies, and TEM indicate that our synthesis procedure results in an exceptionally well ordered purely siliceous MCM-48. Higher quality samples are obtained using synthesis method I and improve further when the surfactant is cethyltrimethylammonium bromide.

Method II provides a guide for predicting the most appropriate conditions for the formation of the hexagonal, cubic, and lamellar phases. The cubic phase is formed when the amount of hydroxide in the gel mixture and the Sfct/Si ratio are high, suggesting that the silicate anion promotes the formation of a liquid-crystal phase. The structure of the mesoporous product is intimately linked to the properties of the surfactant.

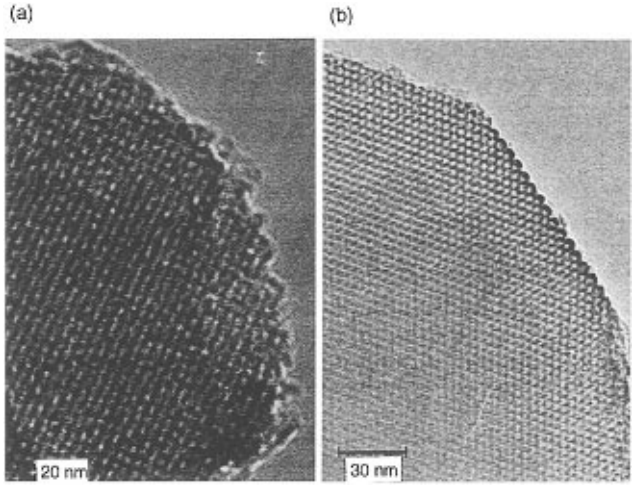

Figure 8. TEM images of sample I-B30-1.2 viewed down the (a) [100] and (b) [110] zone axes of a cubic unit cell with $a = 84$ Å.

Acknowledgment. We are grateful to the European Community for grants to M.D.A. and A.A.R., and to the Departamento de Química Orgánica, Universidad de Córdoba, for enabling us to perform the DRIFT and nitrogen adsorption measurements.

References and Notes

(1) Beck, J. S.; Vartuli, J. C.; Roth, W. J.; Leonowicz, M. E.; Kresge, C. T.; Schmitt, K. D.; Chu, C. T.-W.; Olson, D. H.; Sheppard, E. W.; McCullen, S. B.; Higgins, J. B.; Schlenker, J. L. *J. Am. Chem. Soc.* **1992**, *114*, 10834.

(2) Kresge, C. T.; Leonowicz, M. E.; Roth, W. J.; Vartuli, J. C.; Beck, J. S. *Nature* **1992**, *359*, 710.

(3) Zhao, X. S.; Lu, C. Q.; Millar, G. J. *Ind. Eng. Chem. Res.* **1996**, *35*, 2075.

(4) Sayari, A. *Chem. Mater.* **1996**, *8*, 1840.

(5) Jacobs, P. A.; Martens, J. A. *Synthesis of High-Silica Aluminosilicate Zeolites*; Elservier: Amsterdam, 1987.

(6) Huo, Q.; Margolese, D. I.; Ciesla, U.; Feng, P.; Gier, T. E.; Sieger, P.; Leon, R.; Petroff, P. M.; Schüth, F.; Stucky, G. D. *Nature* **1994**, *368*, 317.

(7) Vartuli, J. C.; Schmitt, K. D.; Kresge, C. T.; Roth, W. J.; Leonowicz, M. E.; McCullen, S. B.; Hellring, S. D.; Beck, J. S.; Schlenker, J. L.; Olson, D. H.; Sheppard, E. W. *Stud. Surf. Sci. Catal.* **1994**, *84*, 53.

(8) Huo, Q.; Leon, R.; Petroff, P. M.; Stucky, G. D. *Science* **1995**, *268*, 1324.

(9) Bagshaw, S. A.; Ponzet, E.; Pinnavaia, T. J. *Science* **1995**, *269*, 1242.

(10) Tanev, P. T.; Pinnavaia, T. J. *Science* **1995**, *267*, 865.

(11) Monnier, A.; Schüth, F.; Huo, Q.; Kumar, D.; Margolese, D.; Maxwell, R. S.; Stucky, G. D.; Krishnamurty, M.; Petroff, P.; Firouzi, A.; Janicke, M.; Chmelka, B. F. *Science* **1993**, *261*, 1299.

(12) Liu, J.; Kim, A. Y.; Virden, J. W.; Bunker, B. C. *Langmuir* **1995**, *11*, 689.

(13) Cheng, C. F.; Luan, Z.; Klinowski, J. *Langmuir* **1995**, *11*, 2815.

(14) Tiddy, G. J. T. *Phys. Lett.* **1980**, *57*, 1.

(15) Blackmore, E. S.; Tiddy, G. J. T. *Liq. Cryst.* **1990**, *8*, 131.

(16) Belmajdoub, A.; Boubel, J. C.; Canet, D. *J. Phys. Chem.* **1989**, *93*, 4844.

(17) Henriksson, U.; Blackmore, E. S.; Tiddy, G. J. T.; Soderman, O. *J. Phys. Chem.* **1992**, *96*, 3894.

(18) Vartuli, J. C.; Schmitt, K. D.; Kresge, C. T.; Roth, W. J.; Leonowicz, M. E.; McCullen, S. B.; Hellring, S. D.; Beck, J. S.; Schlenker, J. L.; Olson, D. H.; Sheppard, E. W. *Chem. Mater.* **1994**, *6*, 2317.

(19) Raman, N. K.; Anderson, M. T.; Brinker, C. J. *Chem. Mater.* **1996**, *8*, 1682.

(20) Sing, K. S. W.; Everett, D. H.; Houl, R. A. W.; Moscou, L.; Pierotti, R. A.; Rouquerol, J.; Siemieniewska, T. *Pure Appl. Chem.* **1985**, *57*, 603.

(21) Barrett, E. P.; Joyner, L. G.; Halenda, P. P. *J. Am. Chem. Soc*. **1951**, *73*, 373.
(22) Schmidt, R.; Stöcker, M.; Akporiage, D.; Tørstad, E. H.; Olsen, A. *Microporous Mater*. **1995**, *5*, 1.
(23) Cullity, B. D. *Elements of X-Ray Diffraction*, 2nd ed.; Addison-Wesley: Reading, MA, 1978.
(24) Little, L. H. *Infrared Spectra of Adsorbed Species*; Academic Press: London, 1966.
(25) Laughlin, R. B.; Joannopoulos, J. D. *Phys. Rev. B* **1977**, *16*, 2942.
(26) Galeneer, F. L.; Leadbetter, A. J.; Stringfellow, M. W. *Phys. Rev. B* **1983**, *27*, 1052.
(27) Bertoluzza, A.; Fagnano, C.; Morelli, M. A.; Gottardi, V.; Guglielmi, M. *J. Non-Cryst. Solids* **1982**, *48*, 117.
(28) Decottignies, M.; Phalippou, J.; Zarzycki, J. *J. Mater. Sci.* **1978**, *13*, 2605.
(29) Soda, I. *Bull. Chem. Soc. Jpn.* **1961**, *34*, 1491.
(30) Durán, A.; Serna, C.; Fornés, V.; Fernández-Navarro, J. M. *J. Non-Cryst. Solids* **1986**, *82*, 69.
(31) Fyfe, C. A.; Gobbi, G. C.; Klinowski, J.; Thomas, J. M.; Ramdas, S. *Nature* **1982**, *296*, 530.
(32) Wu, E. L.; Lawton, S. L.; Olson, D. H.; Rohrman, A. C., Jr.; Kokotailo, G. T. *J. Phys. Chem.* **1979**, *83*, 2777.
(33) Ramdas, S.; Klinowski, J. *Nature* **1984**, *308*, 521.
(34) Engelhardt, G.; Radeglia, R. *Chem. Phys. Lett.* **1984**, *108*, 271.
(35) Zhang, W.; Pinnavaia, T. J. *Catal. Lett.* **1996**, *38*, 261.
(36) Brunauer, S.; Deming, L. S.; Deming, W. S.; Teller, E. *J. Am. Chem. Soc.* **1940**, *62*, 1723.
(37) Luan, Z.; He, H.; Zhou, W.; Cheng, C. F.; Klinowski, J. *J. Chem. Soc., Faraday Trans.* **1995**, *91*, 2955.
(38) Schmidt, R.; Junggreen, H.; Stöcker, M. *J. Chem. Soc., Chem. Commun.* **1996**, 875.
(39) Schmidt, R.; Stöcker, M.; Ellestad, O. H. *Stud. Surf. Sci. Catal.* **1995**, *97*, 149.
(40) Gregg, S. J.; Sing, K. S. W. *Adsorption, Surface Area and Porosity*, 2nd ed.; Academic Press: New York, 1982; p 286.